HHS Public Access

Author manuscript

Exp Eye Res. Author manuscript; available in PMC 2017 April 29.

Published in final edited form as:

Exp Eye Res. 2017 March ; 156: 50–57. doi:10.1016/j.exer.2016.03.009.

The cause and consequence of fiber cell compaction in the vertebrate lens

Steven Bassnett[a,*] and **M. Joseph Costello**[b]

[a]Department of Ophthalmology and Visual Sciences, Washington University School of Medicine, USA

[b]Department of Cell Biology and Physiology, University of North Carolina School of Medicine, USA

Abstract

Fiber cells of the ocular lens are arranged in a series of concentric shells. New growth shells are added continuously to the lens surface and, as a consequence, the preexisting shells are buried. To focus light, the refractive index of the lens cytoplasm must exceed that of the surrounding aqueous and vitreous humors, and to that end, lens cells synthesize high concentrations of soluble proteins, the crystallins. To correct for spherical aberration, it is necessary that the crystallin concentration varies from shell-to-shell, such that cellular protein content is greatest in the center of the lens. The radial variation in protein content underlies the critical gradient index (GRIN) structure of the lens. Only the outermost shells of lens fibers contain the cellular machinery necessary for protein synthesis. It is likely, therefore, that the GRIN (which spans the synthetically inactive, organelle-free zone of the lens) does not result from increased levels of protein synthesis in the core of the lens but is instead generated through loss of volume by inner fiber cells. Because volume is lost primarily in the form of cell water, the residual proteins in the central lens fibers can be concentrated to levels of >500 mg/ml. In this short review, we describe the process of fiber cell compaction, its relationship to lens growth and GRIN formation, and offer some thoughts on the likely nature of the underlying mechanism.

Keywords

Lens; Compaction; Volume control; Refractive index; GRIN; Crystallin; Oncotic pressure

1. Introduction

While humans have usually achieved their full stature and weight by the first years of their third decade, the growth of the ocular lens continues unabated. As first noted by Priestly Smith in the late nineteenth century, both the mass and volume of the human lens increase

*Corresponding author. Department of Ophthalmology and Visual Sciences, Washington University School of Medicine, 660 S. Euclid Ave, MO, 63110, USA. Bassnett@vision.wustl.edu (S. Bassnett).

The authors would like to dedicate this article to the memory of Dr. David Beebe. Dave's contribution to the field of lens and vision research was considerable. His boundless curiosity, enthusiasm and good humor were an inspiration to everyone fortunate enough to make his acquaintance. Dave was interested in many aspects of ocular biology, not least the origin of the lens refractive index gradient. We miss him dearly.

steadily, until the very end of life (Smith, 1882, 1883). The continuous addition of newly differentiated cells to the lens surface is, to a large degree, offset by the gradual compaction of pre-existing cells in the body of the lens. The compaction process is difficult to visualize directly, but at the cellular level, must involve a significant loss of volume and accompanying changes in fiber cell morphology. Fiber cell compaction is necessary to prevent the lens from overgrowing the eye (which, in humans, achieves its maximum external dimensions in early childhood (Augusteyn et al., 2012)) and also has an important role in the optical development of the lens. In most species, the refractive index of lens fiber cell cytoplasm varies as a parabolic function of the lens radius, being greatest in the lens nucleus. The resulting gradient refractive index (GRIN) contributes to the dioptric power of the lens, while minimizing positive spherical aberration. The GRIN spans the organelle-free zone (OFZ) of the lens. Because cells in this region lack the capacity for protein synthesis (Faulkner-Jones et al., 2003), the increase in cytoplasmic protein concentration in the inner cell layers cannot be attributed simply to the production of new protein. Instead, it may be secondary to the removal of water from the cytosol during the compaction process.

2. The lens grows by a process of accretion

The fundamental growth process of the lens is reasonably well understood. The lens cell population is contained within a thick basement membrane, the capsule. The majority of the lens volume is filled by fiber cells arranged in a series of concentric lamellae. The anterior surface of the fiber cell mass is covered by an epithelium. Near its equatorial margin, beneath the attachment points of the zonular fibers (Shi et al., 2013), is a band of epithelial cells called the germinative zone (GZ; (Harding et al., 1960)). Studies in the 1960's demonstrated that S-phase cells are largely restricted to the GZ which, consequently, can be thought of as the fundamental growth engine of the lens. Proliferation of GZ cells results in the progressive displacement of epithelial cells into the fiber cell compartment. Cell death is rare in the healthy lens epithelium (Shi et al., 2015; Takamura et al., 2003), and given that the surface area of the lens increases several fold during postnatal development, the epithelial cell population is surprisingly constant (Shi et al., 2015). Under these conditions, at least over a short interval, the number of epithelial cells produced by mitosis in the GZ must equal the number of fiber cells deposited in the body of the lens. This realization forms the basis of the “penny pusher” model of lens growth (Shi et al., 2015). The quantitative relationships between epithelial cell density, mitotic index, and radial lens growth have also been explored mathematically (Sikic et al., 2015; Wu et al., 2015). Mitotic index varies not only with latitudinal location within the epithelium (being highest in the GZ and virtually zero in the central epithelium) but also with age. In two-week-old mice, for example, the peak S-phase labeling index in the GZ is ≈ 7%, a value that falls to ≈ 2% in aged lenses (Shi et al., 2015). This decline is reflected in the reduced rate of macroscopic lens growth at later ages observed in many species (as discussed below, the linear postnatal growth of the human lens is an exception in this regard).

At the lens equator, epithelial cells withdraw from the cell cycle, become aligned in meridional rows, and begin the process of fiber cell differentiation (Mochizuki and Masai, 2014). Fiber differentiation is characterized most obviously by an enormous increase in cell length (to values approaching 2 cm in the large bovine lens (Kuszak et al., 2004)). However,

the initial stage of elongation (when fiber cells have yet to reach 100 μm in length) is accomplished through a change in shape (to a flattened, ribbon-like form) rather than a volume increase (Bassnett, 2005). At later stages, volume increases in proportion to length (Bassnett and Winzenburger, 2003). The differentiation process is continuous. By the time the tips of fiber cells converge with those projecting from the opposite hemisphere of the lens (at the sutures), their mid-regions have already become covered by many layers of more recently differentiated fiber cells.

3. Patterns of macroscopic lens growth

All vertebrate lenses increase in mass throughout life but there are interesting differences in lens growth kinetics between species. Lens growth in humans is characterized by rapid, asymptotic growth during gestation and the first few postnatal years, followed by slow but constant growth throughout the remainder of the lifespan (Augusteyn, 2007). By the end of the first postnatal year, the human lens weighs about 150 mg (Augusteyn, 2007). Thereafter, growth slows to a linear rate of 1.38 mg/year. In contrast to the biphasic growth of the human lens, the increase in lens weight in most species is monophasic and well described by a logistic equation of the form $W = W_m e^{-(k/A)}$, where W is lens weight, W_m is maximum asymptotic weight, k is the logistic growth constant, and A is time from conception (Augusteyn, 2014a).

4. Evidence of fiber cell compaction

Given that lenses grow steadily throughout life, there seems no reason, a priori, to suspect that fiber cell compaction (i.e., cell shrinkage) might be occurring at the same time. However, a “backof-the-envelope” calculation can show that compaction probably must occur if the lens is to fit comfortably within the eye ball. We can calculate the rate at which lens volume would be expected to increase in the absence of compaction. For example, the lens of a 1-year-old C57Bl6 mouse has a radius of 1270 μm (Shi et al., 2015). At that age, the lens epithelium contains approximately 43,000 cells of which, at any time, ≈ 200 are in S-phase of the cell cycle (Shi et al., 2015). In mouse lenses, S-phase reportedly lasts 12 h (Rafferty and Smith, 1976). Thus, ≈ 400 new cells are produced by the epithelium each day. Cell death is undetectably low in this population. Consequently, the fate of new daughter cells will be to differentiate into fiber cells (thereby increasing lens volume and surface area) or be incorporated into the epithelial cell population (facilitating the expansion of the epithelium necessary to cover the growing surface). Using a quantitative growth model (Sikic et al., 2015), we can apportion the cells between the two fates. We calculate that of the 400 newly-produced cells, on average, 58 will be added to the epithelium each day, while 342 cells will differentiate into fibers. In adult lenses, newly formed fiber cells have a flattened hexagonal cross section, with dimensions of ≈ 10 × 2 μm (area ≈ 20 μm^2). Geometry shows that, after an additional year of growth, the lens radius should have increased to 1550 μm. By the end of the mouse lifespan (in our lab, ≈ 3.5 years), the radius should have increased to >1900 μm. In fact, these estimates substantially overshoot empirical measurements, where the radius of the aged lens is only ≈ 1300 μm. Expressed in terms of lens volume, the discrepancy is approximately ≈ 3-fold. Thus, it is difficult to

model lens growth accurately (particularly at later stages) without including cell compaction as a key model parameter.

Through careful clinical observation, the process of central compaction can be visualized directly in human patients. Certain pathological conditions cause discrete regions of the lens to become opaque. Physical trauma to the eye, for example, may result in opacification of a thin layer of fiber cells located immediately beneath the lens epithelium (Brown, 1976). As normal growth resumes, the opaque layer is buried progressively by layers of healthy, transparent fiber cells. Similarly, some congenital cataracts affect the nuclear or perinuclear regions only, with postnatal lens growth proceeding quite normally (Brown et al., 1988). This allows the size and shape of the opaque nucleus to be visualized over the succeeding years or even decades. With time, the distance between localized opacities and the lens surface increases. Early investigators assumed that the increase was due to the deposition of new fiber cells on the lens surface. Indeed, efforts were made to date the occurrence of a cataract by simply measuring its depth below the lens surface, an approach known as phakochronology (Bellows, 1968). Thus, for example, if the lens increased in sagittal width at a rate of 28 μmper year (14 μm of new cells being added to the anterior cortex of the lens and 14 μm to the posterior cortex) and the opacity was located 42 μm below the anterior surface, then the cataract was presumed to have formed three years (42/14 = 3) earlier. Intriguingly, however, long-term Scheimpflug imaging studies on patients revealed that localized opacities receded into the lens at a rate that exceeded (by as much as 50%) the measured growth rate (Brown, 1976, 1977; Brown et al., 1988). On the basis of this observation it was concluded that two processes must be occurring concurrently: addition of fiber cells to the surface and compaction of the inner cells. Further, by measuring independently the fate of nuclear (Brown et al., 1988) and cortical (Brown, 1976) opacities, regional compaction rates could be computed. Nuclear compaction occurred most rapidly in young lenses, declining to a slow, relatively steady rate by the end of adolescence. The rate of cortical compaction did not vary significantly with age but was, at all ages, most rapid for opacities located in the outer cell layers. Thus, in vivo observations on the human lens suggested that fiber cell compaction is initiated in the lens nucleus but, by middle age, the phenomenon is largely restricted to the lens cortex.

Measures of the relative rates of accumulation of wet weight and dry weight have been taken as evidence of lens fiber cell compaction. Logistic analysis of growth rates in a number of species indicates that lens dry weight generally increases more rapidly than wet weight (Augusteyn, 2014a). In rat lenses, for example, the dry/wet weight ratio approaches an asymptotic value of ≈ 0.6 (Augusteyn, 2014b). The increasing proportion of dry weight is consistent with the idea that fiber cells shrink over time and that volume loss is primarily in the form of water. Measurements with impermeant tracers such as ^{14}C-inulin and ^{14}C-mannitol indicate that only a small fraction (1–5%) of lens water is located extracellularly (Yorio and Bentley, 1976), so dehydration likely involves removal of water from the cytosol rather than the extracellular space. Certainly, the absolute water content in the outer cell layers is much greater than in the center of the lens (85% vs 58% in human lenses) as shown, for example, by Raman micro-spectroscopy (Siebinga et al., 1991). It is possible that compaction may also involve some loss of dry mass, but if this were the case, cells would have to lose a greater fraction of their volume to achieve a given cytoplasmic protein

concentration. Birds and reptiles represent an interesting counter example because in their lenses the proportion of dry weight remains relatively constant over time. This may indicate that lens compaction does not occur in these groups, a notion supported by the results of microscopic and biochemical analyses (see below). In human lenses, the proportion of dry weight increases from 17.8% at 4 months of gestation (Bours and Fodisch, 1986) to 32% at 6-years-of-age. During adulthood, the proportion of dry weight increases only gradually, reaching a maximal value of ≈ 36% in the lenses of nonagenarians (Augusteyn, 2010).

5. Relationship between compaction and GRIN formation

In a lens of uniform composition, light is refracted at the surfaces, according to Snell's law of refraction. The composition of living lenses is generally not uniform, however. All mammalian lenses examined have an internal refractive index (n) gradient, with a significantly higher index in the center of the lens than near the surface (Pierscionek and Regini, 2012). In a rat lens, for example, $n = 1.38$ in the outer layers and $n = 1.50$ in the center of the tissue (Campbell, 1984). The optical consequence of such a gradient index (GRIN) is to cause light rays to bend as they pass through the lens substance. Such a phenomenon can be confirmed visually, by observing the curved path of a collimated beam as it traverses the lens tissue (Axelrod et al., 1988).

The structure of the GRIN can be deduced using various approaches, including ray tracing (Campbell, 1984), reflectometry (Pierscionek,1997), magnetic resonance imaging (Jones et al., 2005) and, most recently, X-ray Talbot interferometry (Hoshino et al., 2011). For most species, the results of such analyses indicate that the gradient has an approximately parabolic form (Hoshino et al., 2011). An exception may be the human lens, where although the GRIN is initially parabolic, with age, a central plateau develops, flanked by shoulder regions wherein the gradient falls steeply (Moffat et al., 2002; Pierscionek et al., 2015). The resulting index distribution is best fitted by a higher order parabolic function or a power law function (Pierscionek et al., 2015).

The contribution of the GRIN to the refractive power of the lens can be expressed through the concept of equivalent refractive index. The equivalent refractive index is calculated by measuring the focal length of a lens, its thickness, and the curvature of its surfaces, and then computing the corresponding refractive index for a lens of uniform composition. Typical values for the equivalent refractive index of the human lens range from $n = 1.426–1.441$ (Dubbelman and Van der Heijde, 2001; Glasser and Campbell, 1999; Mutti et al., 1995). The actual refractive index of the central, plateau region of the human lens has been measured using optical techniques, yielding values in the range $n = 1.402$ (Pierscionek, 1997) −1.418 (Augusteyn et al., 2008) Near the lens surface the index falls to $n = 1.381$ (Pierscionek, 1994). The GRIN structure thus contributes to the focusing power of a lens. To achieve the same refractive power as a GRIN lens, the index of a lens of uniform composition would need to be substantially higher at all radial locations, even the nucleus. Assuming that the refractive index is directly proportional to the protein concentration within a cell, the presence of the GRIN structure has the further (and beneficial) effect of reducing the amount of protein that lens fiber cells must synthesize to achieve a given dioptric power. Moreover, in the absence of a GRIN, the concentration of protein needed to achieve the necessary

focusing power might be so high that the viscoelastic properties of the lens tissue would be altered significantly. For species, like humans, that adjust the shape of the lens to focus on near or distant objects, substantially higher protein concentrations in the cortical layers would likely affect the speed of accommodation.

The GRIN contributes not only to the effective optical power of a lens but also, importantly, to its quality. In lenses of uniform composition, optical performance is often degraded by the presence of positive spherical aberration. In such a system, paraxial rays (those rays passing close to the optical axis of the lens) are less strongly refracted than marginal rays (those rays furthest from the optical axis) resulting in a poorly focused image. Living GRIN lenses, particularly those of marine organisms (where the lens is the primary focusing element), are often exquisitely well corrected for spherical aberration (Kreuzer and Sivak, 1984; Sivak et al., 1994).

From a mechanistic perspective, it is of interest to determine whether the GRIN structure is in place from the time of lens inception or instead emerges later in development. This issue has been examined in the fetal bovine lens (Pierscionek et al., 2003). At approximately nine months, the gestation period in cows is close to that of humans. For the first half of gestation, reflectometric measurements suggest that the refractive index of the fiber cell cytoplasm is relatively uniform. However, beginning at about 4.5 months of gestation, the characteristic parabolic GRIN structure emerges, with high ($n \approx 1.43$) refractive index values in the lens core and lower values (≈ 1.36) closer to the surface. For many animals, high acuity vision is required from the moment of birth. It is not perhaps surprising, therefore, that the GRIN is in place before the end of gestation.

Once formed, the GRIN is remarkably stable in the face of continuous tissue growth. However, in aged human lenses there is some evidence that the GRIN begins to degenerate, with decentration of the index contours and a slight decrease in the maximal index value in the center of the lens (Pierscionek et al., 2015).

It is accepted that the refractive index of the lens cell cytoplasm is a direct function of the cytoplasmic protein concentration, the relationship between the two being specified by the Gladstone–Dale formula (Gladstone and Dale, 1864), in the form introduced by Barer and Joseph (Barer and Joseph, 1954),

$$n = n_s + \Delta c, \quad (1)$$

where n is the refractive index of the solution, n_s is the refractive index of the solvent, Δ is the specific refractive index increment (ml/g) and c is protein concentration (g/ml). The refractive index increment (also referred to as dn/dc) refers to the rate of change of the refractive index with concentration for a sample at a given temperature, a given wavelength, and in a given solvent. It is often assumed that all proteins have the same dn/dc but this is not quite accurate (Zhao et al., 2011b). In silico analysis of the set of proteins encoded by the human genome suggests a mean dn/dc value of 0.1899. Interestingly, crystallins in general exhibit higher values (mean 0.1930 ml/g) and γ-crystallins, which are especially

abundant in the lens nucleus, have the highest dn/dc values (0.1969–0.2000) of all (Zhao et al., 2011a). By expressing proteins with unusually high dn/dc values, lens cells are able to achieve a given refractive power at lower protein concentrations.

The Gladstone–Dale formula allows the GRIN structure to be deduced directly from the radial distribution of protein or the converse. In the rat lens, for example, the variation of protein concentration with depth has been determined (Philipson, 1969) and the relative expression levels of α-, β-, and γ-crystallins (along with their respective dn/dc values) in the central and peripheral layers are known (Pierscionek et al., 1987). The radial variation in refractive index distribution calculated using these data is a close fit to the GRIN deduced from ray tracing measurements (Campbell, 1984).

6. Morphological/cellular correlates of the compaction process

Results of growth modeling, in vivo imaging, shifting dry weight/wet weight ratios, and analysis of water and protein concentration gradients are consistent with the idea that lens fiber cells undergo significant volume loss over time. What, if any, are the morphological correlates of this process?

In order to quantify the process of fiber volume loss it would be helpful to follow the volume of specified cells over time. Such an analysis is not yet practicable. However, measurements of the cross sectional areas of cells located at specified points on the lens radius have been reported. For example, in the rabbit lens, the cross sectional area of fiber cells located 7 mm from the lens center decreased from 17.31 μm^2 in 1.5-year-old animals to 8.98 μm^2 in 4-year-old animals, a 48% reduction (Al-Khudari et al., 2007). It is worth noting that due to volume loss in the inner cells, the cells located 7mm from the center of the young lens are not the same as those located 7 mm from the center of the old lens. Nevertheless, the trend is toward a marked reduction in the cross sectional area of cortical fiber cells over time.

In human lenses, one cell population that can be identified unambiguously is that of the embryonic nucleus (EN). The human EN (comprising the primary fiber cells) consists of ≈ 800 cells located in the center of the tissue and oriented along the optic axis (Taylor et al., 1996). Unlike the crescent-shaped fiber cells found elsewhere in the lens, the fibers of the EN are relatively straight. A comparative analysis of EN cell length in young (15–25 years-of-age) and old (59–81 years-of-age) donors suggests that this fiber population becomes significantly shorter over time. Furthermore, in older lenses, accordion-like “compaction folds” form in the EN cell membranes, oriented orthogonal to the long axis of the cells (Al-Ghoul et al., 2001). The shortening of the EN cells is accompanied by a corresponding decrease in the elliptical angle of cells in the surrounding fetal nucleus.

Compaction folds are a feature of EN cells, but a second type of surface “wrinkling”, morphologically distinct from the compaction folds, is also observed. First described in primate lenses as “tongueand-groove” junctions (Dickson and Crock, 1972) and later as “furrowed membranes” (Kuszak et al., 1988), these pleats in the fiber cell plasma membrane are present in all mammalian species (al-Ghoul and Costello, 1993; Al-Ghoul et al., 2001; Freel et al., 2003; Kuszak and Costello, 2004; Kuszak et al., 1988; Kuwabara, 1975; Lo et

al., 2014; Lo and Harding, 1984; Taylor et al., 1996; Vrensen et al., 1992). More properly referred to as microplicae, the membrane folds are detected initially in the inner cortical fiber cells and become increasingly numerous with depth, completely covering the surface of the nuclear fibers. The close apposition of the plasma membranes of neighboring cells ensures that the topology of the microplicae on one cell is matched by a complementary series of folds on the neighboring cell. Freeze fracture images have revealed the presence of intramembranous particles in the microplicae. The particles (composed of an integral membrane protein called AQP0) are arranged in square array domains that are particularly numerous in the convex portion of the folded membrane (Costello et al., 1985, 1989; Lo and Harding, 1984; Zampighi et al., 1982, 1989). By contrast, the concave portions of the folds are protein poor. Thus, square arrays in the membrane of one cell are located opposite protein poor regions in the membrane of the adjacent cell. It is not yet evident whether the offset expression of square array domains is a cause or a consequence of microplicae formation.

Fiber cells in the inner regions of the lens lack all organelles, including the endoplasmic reticulum, Golgi apparatus and the machinery necessary for trafficking of membrane vesicles. In the absence of these organelles, it is difficult to envisage how the plasma membrane of mature fiber cells could be remodeled. If the surface area of a cell located within the OFZ is indeed constant, then a marked loss of cell volume will inevitably cause the membrane to become folded. Thus, the presence of compaction folds in the center of the human lens and the presence of microplicae in nuclear fiber cell membranes of many species are consistent with the notion that cell volume is lost while membrane area is conserved. Once again, a potentially informative counter example is the avian lens. In birds, the cross sectional shapes of the fiber cells do not change significantly with depth and microplicae are absent from the inner cells (Kuszak et al., 1980; Stirling and Wakely, 1987; Willekens and Vrensen, 1985). As mentioned earlier, the proportion of dry weight in the bird lens remains relatively constant with age, suggesting that fiber cell compaction does not occur. It could be a coincidence that the absence of lens compaction is accompanied by the absence of microplicae but these observations are certainly consistent with the hypothesis that microplicae formation is a result of fiber cell volume loss.

In adult human lenses, the refractive index rises sharply in the outer 0.5–1.0 mm of tissue and then remains relatively constant across most of the lens radius (Pierscionek et al., 2015). It is of interest to examine the morphology of cells located in the peripheral tissue, where the index is changing most rapidly (see Fig. 1). The outer 75 μm of lens tissue contains fiber cells with a typical flattened hexagonal appearance in cross section (Fig. 1A). The cells are aligned in radial cell columns (Fig. 1B), contain organelles, and have relatively smooth membranes and lightly stained cytoplasm (Costello et al., 2013). However, at a depth of 75–100 μm, the regular hexagonal organization breaks down abruptly and the plasma membranes become extremely irregular, with numerous finger-like projections extending from the cells. The cellular morphology changes so dramatically in this region that it is difficult to recognize the original flattened hexagonal shape. Remarkably, these massive changes in shape occur without disturbing the structure of gap junctions and while maintaining cellular integrity. This region, which is visible by light or electron microscopy, is barely 40 μm wide and has been called the remodeling zone (Lim et al., 2009). As cells

exit the remodeling zone, they lose their organelles and have a more densely stained and finely textured cytoplasm (Fig. 1C), suggesting that compaction has commenced. Between the remodeling zone and the surface of the adult nucleus, some 400–500 μm further into the lens, the cells become increasingly flattened (Taylor et al., 1996). The cross sectional area of cortical cells located <100 μm into the lens is 24 μm^2, while cells in the adult nucleus have an area of 7 μm^2. Compaction in the adult nucleus appears to be age dependent. In lenses from 90-year-old donors, fiber cell thickness is reduced to ≈ 0.4 μm, giving a nominal cross sectional area of 4 μm^2 (Costello et al., 2013). Modifications to the cytoskeleton and membrane skeleton within the remodeling zone may release integral membrane proteins, allowing AQP0 to self-associate in the membrane plane to form square arrays. The square arrays run along the ridges and furrows of the microplicae that first begin to appear about 50 μm deeper than the remodeling zone (Costello et al., 2013).

If the refractive index distribution within the lens is an accurate reflection of cell volume loss, then we might expect to observe a radial distribution of cross sectional areas that mirrors the index profile. In the human lens at least, this is not observed. As mentioned above, there is compelling evidence of cell compaction in the region between the lens surface and the adult nucleus 600–700 microns into the lens. However, within the central plateau region, where the index is constant, a range of cell profiles are observed. Indeed, the cells with the largest cross sectional area are found in the EN located in the center of the adult lens. The simplest explanation for this apparent discrepancy is that the cross sectional area of newly differentiated fiber cells varies. From the perspective of GRIN formation the final area of the cell is irrelevant. It is only necessary that the cell loses sufficient volume to cause the necessary increase in protein concentration and refractive index. In adult lenses, the central EN cells have a cross sectional area of ≈ 80 μm^2 (Taylor et al., 1996). We do not yet know what the cross sectional area of the EN cells was when they first differentiated early in development, but it is not inconceivable that the value was two- or three-fold greater than at later stages.

7. Mechanism of compaction

Although it is possible to conceive of external forces acting upon the lens to cause loss of fiber cell volume in the lens interior, it seems more plausible to posit that mechanisms intrinsic to the fiber cells themselves are in play. Of these, we can distinguish between energy-consuming, largely membrane-based mechanisms and passive mechanisms arising from the inherent physical properties of the crystallin proteins themselves.

All cells actively regulate their volume and lens cells are no different. If an intact lens is placed in a hypotonic solution it swells initially, before slowly regaining its original volume through regulatory volume decrease, a process involving loss of loss of K^+, Cl^-, and ultimately water (Patterson and Fournier, 1976). Similarly, regulatory volume increase (achieved through accumulation of Na^+, K^+ and Cl^-) serves to reverse lens shrinkage caused by exposure to hypertonic solutions. Under normal circumstances, the lens maintains a constant volume, but the same cannot be said for its component cells. The outer fiber cells (comprising perhaps 20% of the radius) are in the process of actively elongating (and thus

increasing in volume) while many of the inner cells are undergoing fiber cell compaction (and thus decreasing in volume).

All cells contain significant amounts of high molecular weight anionic colloids (mostly proteins) to which the plasma membrane is impermeable. In contrast, the extracellular solution (in this case the aqueous humor) contains relatively little colloid. Under these conditions, if nothing were to intervene, a Gibbs–Donnan equilibrium would be established across the membrane, electroneutrality would be achieved in the extracellular and intracellular compartments, and the osmolarity within the cell would exceed that of the surrounding fluid. In response to the osmotic pressure differential, water would move into the cell down its concentration gradient and the cell would swell and eventually burst. The fact that cells evidently avoid this fate is largely attributable to the action of the Na/K-ATPase (embedded in a plasma membrane that is relatively impermeable to sodium but permeable to potassium). The activity of the Na/K-ATPase maintains a transmembrane gradient of cations that generates a negative internal potential. The negative membrane potential allows a low concentration of intracellular Cl^- to be in electrochemical equilibrium with much higher concentrations of extracellular Cl^-. Thus, the osmotic pressure generated by anionic colloid is ultimately offset by the exclusion of Cl^- from the cytosol.

The lens is a syncytial tissue in which the routes for sodium efflux and influx are spatially segregated. Lens Na/K-ATPase is concentrated in the equatorial epithelium, while sodium “leak” channels (perhaps comprised of connexin hemichannels (Ebihara et al., 2014)) are located in the plasma membranes of inner fiber cells. This arrangement leads to the generation of a circulating sodium current (Mathias, 1985). The bulk flow of water that accompanies the movement of sodium through the lens is thought to constitute an internal microcirculation system which convects nutrients to the inner cells and removes waste metabolites (Mathias et al., 2007). According to this model, sodium diffuses into the lens at the poles and moves into the tissue via the extracellular space before crossing the inner fiber cell membranes. The local osmotic gradient created by the sodium influx draws water into the cells. In the return leg of the circuit, sodium and water move from cell-to-cell (via the extensive system of gap junctions that interconnects the fiber cells) before exiting at the lens equator. Because gap junction channels offer some resistance to the bulk flow of water, a radial hydrostatic pressure gradient develops, with a mean central value of 335 mm/Hg, which falls to 0 mm/Hg immediately beneath the lens surface (Gao et al., 2011, 2013). The pressure gradient has a parabolic form reminiscent of the GRIN and indeed it has been suggested that the bulk flow of water may play a role in establishing the index gradient (Gao et al., 2013, 2015). In support of an active role for the lens microcirculation in generating and maintaining the GRIN, MRI imaging has been used to demonstrate that in the presence of high potassium solutions, low temperature, or ouabain (an inhibitor of the Na/K-ATPase), the water-protein gradient of the lens collapses and negative spherical aberration is reduced leading to reduced image quality (Vaghefi et al., 2011, 2015). On the basis of these findings it was concluded that the protein concentration gradients that underlie the GRIN are actively maintained through membrane-based processes. The precise mechanism by which the hydrostatic pressure gradient might shape the refractive properties of the lens remains obscure, however. It is possible that the microcirculation plays a role in controlling the

overall volume of the lens syncytium rather than determining how that volume is apportioned among the various cellular compartments.

Interestingly, certain genetic manipulations have been shown to modulate lens hydrostatic pressure. For example, knockout of one allele of the *Cx46* gene leads to a striking increase in hydrostatic pressure, to values nearly twice that of wildtype lenses (Gao et al., 2011). Conversely, when *Cx46* is knocked into the *Cx50* locus, cell–cell coupling doubles and this is associated with a 50% reduction in the hydrostatic pressure gradient. In light of these observations, it would be of considerable interest to determine whether the structure of the GRIN is significantly altered in the connexin hemizygous and knockin lenses which are, in other respects, indistinguishable from wildtype (Mathias et al., 2010).

Membrane-based mechanisms may play a role in GRIN formation. The alternative hypothesis, that radial concentration gradients might arise spontaneously through the intrinsic properties of the crystallin proteins was first proposed by Vérétout and Tardieu (Veretout and Tardieu, 1989) and is outlined in a slightly modified form here. This explanation depends on the colloid osmotic properties of the fiber cell cytoplasm. A colloid is a suspension in which the finely dispersed particles do not settle out over time. A protein solution can be considered a colloid (although a strict chemical definition of colloid often excludes true solutions). Colloid osmotic pressure or “oncotic” pressure is a familiar concept in the field of hemodynamics. In the bloodstream, albumin is the most important colloid and exerts the greatest oncotic pressure. The effect of oncotic pressure is to cause fluid to be drawn back into vessels at the venous end of capillary beds (the fluid having been expelled from the arterial end of the capillary by hydrostatic pressure generated through the pumping action of the heart). Colloids generally make only a small contribution to the total osmotic pressure of a solution such as blood because the oncotic pressure is overwhelmed by the contribution of the other solutes. In plasma, for example, the oncotic pressure is only ≈ 0.5% of the total osmotic pressure. However, osmotic and oncotic pressures are always measured relative to a specified membrane. If two colloidal solutions are separated by a membrane that is permeable to water and small solutes but impermeable to protein, then the oncotic pressure is the only pressure present. Oncotic pressure (Π) can be determined empirically in an oncometer or calculated using the van't Hoff equation,

$$\Pi = i(M)RT \quad (2)$$

where i is the van't Hoff factor (i.e., the number of particles into which a substance dissociates), M is molarity, R is the gas constant and T is temperature (in °K).

To understand how oncotic pressure could influence the volume of fiber cells located near the center of the lens let us briefly recall that lens cells are organized in a series of lamellae. In a one-year-old mouse, for example, the radius of the lens is approximately 1200 μm and the width of an individual fiber cell is ≈ 2 μm, suggesting that ≈ 600 cell layers are present. The layers are well connected by gap junctions; channels that facilitate the intercellular movement of water and small metabolites with molecular weights of less than 1 kDa. Significantly, proteins are unable to diffuse through the gap junctions. Thus, with respect to

the redistribution of water between cells located in adjacent lamellae, small differences in oncotic pressure will be relevant because the other solutes can pass easily through the connecting gap junctions. Measurement of oncotic pressure in homogenates prepared from cortical or nuclear regions of the lens has demonstrated that for a given protein concentration, the oncotic pressure is generally greatest in cortical samples (Veretout and Tardieu, 1989) and the behavior of crude lysates mirrors combinations of purified proteins (Kenworthy et al., 1994). Why would the oncotic pressure differ for cells located at various depths into the lens? There are at least two possibilities. It is known that the ratio of α-to γ-crystallin synthesized by nuclear fiber cells differs significantly from that expressed by cortical fiber cells (γ-crystallin being a particularly abundant protein in the lens nucleus) (McAvoy, 1978; Pierscionek et al., 1987). Thermodynamic measurements on γ-crystallin suggest that repulsive interactions between particles dominate, while for α-crystallin interactions are generally attractive in nature (Veretout et al., 1989). A consequence of this behavior is that solutions of α- or γ-crystallin can deviate significantly from the ideal behavior formalized in the van't Hoff law. Thus, to reduce the volume of a γ-crystallin-rich inner cell it may be sufficient to merely connect it via gap junctions to an αcrystallin-rich outer cell. It is noteworthy that avian lenses, which do not undergo fiber cell compaction, express δ-crystallin rather than γ-crystallin (Wistow and Piatigorsky, 1987).

In addition to qualitative differences in crystallin composition between inner and outer lens fiber cells, quantitative differences exist also. Enzyme-mediated truncation of crystallin proteins is widespread in the developing lens nucleus. In rats, cows and chickens, N-terminal extensions of β-crystallins are removed during the maturation of the lens nucleus through the combined activities of m-calpain (calpain 2) and Lp82 (calpain 3) (David et al., 1994; Shih et al., 1998; Wilmarth et al., 2004). Calpains also appear to be responsible for the removal of C-terminal extensions from α-crystallins (Ueda et al., 2002). Loss of hydrophilic, solvent-exposed C-terminal extensions leads to progressive insolubilization of the truncated protein. Interestingly, calpain activity is not evenly distributed across the lens. In rats, Lp82 is particularly active in the lens nucleus (Ma et al., 1998, 1999) whereas, in mice, calpain 3 is expressed specifically in the deep cortex, where calpain activation precedes loss of the fiber cell organelles (De Maria et al., 2009). It is difficult to quantify the magnitude of such effects but it is likely that on balance the processes of truncation and insolubilization will reduce the oncotic pressure of the inner cell layers.

In summary, radial gradients in oncotic pressure are likely to be established in the lens due to the differential synthesis of crystallin proteins and/or truncation and aggregation phenomena and the net effect will be to reduce the effective particle number in the innermost fiber cells. Such effects, expressed through the semi-permeable membrane provided by the gap junction channels are expected to cause the inner cells to lose water (and thus volume) until their oncotic pressure equilibrates with that of the overlying cells.

There are many unanswered questions. For example, what determines the maximal refractive index and why does this vary between species. In the human lens, for example, the maximal index value in the center of the lens ($n \approx 1.43$) is significantly lower than that of the rodent lens ($n > 1.5$). Clearly volume loss cannot continue indefinitely, but why does it proceed further in some lenses than others? Is this perhaps a reflection of the hydration properties of

the different crystallins? Differential scanning calorimetry measurements allow the proportion of non-freezable water in the cytoplasm to be determined. Non-freezable water is found in the hydration layer at the protein surface. In rats, the non-freezable water in the lens nucleus is ≈ 25% of the total (Castoro and Bettelheim, 1986), while in young humans lenses, the value is close to 46% (Lahm et al., 1985). Perhaps the hydration layer surrounding the nuclear proteins, which in turn is a reflection of their tertiary structure, sets an upper limit to the degree of compaction. Measurements on developing bovine lenses indicate that the GRIN forms approximately midway through gestation (Pierscionek et al., 2003). What process might initiate fiber cell compaction in the central cells at that particular stage of development? Finally, how can we reconcile putative gradients of oncotic pressure with the measured hydrostatic gradient generated as a consequence of the lens microcirculation?

8. Concluding remarks

The gradual loss of cell volume in the inner regions of the vertebrate lens would not appear to be a very consequential process. Yet, without it, the lens could not fit within the eye and the GRIN, so necessary for clear vision, would be absent. Here, we hypothesized that volume loss may be due to the oncotic pressure differential generated between adjacent lens growth shells. If this can be verified, it will establish a link between transcriptional regulation in differentiating fiber cells and the overall optical performance of the lens.

Acknowledgments

This work was supported by National Institute of Health Grant R01 EY09852 and R01 EY024607 (SB), R01EY008148 (MJC), and an unrestricted grant to the Department of Ophthalmology and Visual Sciences from Research to Prevent Blindness. The authors would like to thank Drs. Hrvoje Šikić, Barbara Pierscionek, Richard Mathias, and George Thurston for their helpful comments and suggestions on an earlier version of this manuscript.

References

al-Ghoul KJ, Costello MJ. Morphological changes in human nuclear cataracts of late-onset diabetics. Exp. Eye Res. 1993; 57:469–486. [PubMed: 8282033]

Al-Ghoul KJ, Nordgren RK, Kuszak AJ, Freel CD, Costello MJ, Kuszak JR. Structural evidence of human nuclear fiber compaction as a function of ageing and cataractogenesis. Exp. Eye Res. 2001; 72:199–214. [PubMed: 11180969]

Al-Khudari S, Donohue ST, Al-Ghoul WM, Al-Ghoul KJ. Age-related compaction of lens fibers affects the structure and optical properties of rabbit lenses. BMC Ophthalmol. 2007; 7:19. [PubMed: 18096063]

Augusteyn RC. Growth of the human eye lens. Mol. Vis. 2007; 13:252–257. [PubMed: 17356512]

Augusteyn RC. On the growth and internal structure of the human lens. Exp. Eye Res. 2010; 90:643–654. [PubMed: 20171212]

Augusteyn RC. Growth of the eye lens: I. Weight accumulation in multiple species. Mol. Vis. 2014a; 20:410–426. [PubMed: 24715758]

Augusteyn RC. Growth of the eye lens: II. Allometric studies. Mol. Vis. 2014b; 20:427–440. [PubMed: 24715759]

Augusteyn RC, Jones CE, Pope JM. Age-related development of a refractive index plateau in the human lens: evidence for a distinct nucleus. Clin. Exp. Optom. 2008; 91:296–301. [PubMed: 18201223]

Augusteyn RC, Nankivil D, Mohamed A, Maceo B, Pierre F, Parel JM. Human ocular biometry. Exp. Eye Res. 2012; 102:70–75. [PubMed: 22819768]

Axelrod D, Lerner D, Sands PJ. Refractive index within the lens of a goldfish eye determined from the paths of thin laser beams. Vis. Res. 1988; 28:57–65. [PubMed: 3413999]

Barer K, Joseph S. Refractometry of living cells. I. Basic principles. Q. J. Microsc. Sci. 1954; 95:399–423.

Bassnett S. Three-dimensional reconstruction of cells in the living lens: the relationship between cell length and volume. Exp. Eye Res. 2005; 81:716–723. [PubMed: 15963502]

Bassnett S, Winzenburger PA. Morphometric analysis of fibre cell growth in the developing chicken lens. Exp. Eye Res. 2003; 76:291–302. [PubMed: 12573658]

Bellows JG. Phakochronology. The study of dating structural changes in the lens. Br. J. Ophthalmol. 1968; 52:540–545. [PubMed: 5724441]

Bours J, Fodisch HJ. Human fetal lens: wet and dry weight with increasing gestational age. Ophthalmic Res. 1986; 18:363–368. [PubMed: 3601352]

Brown N. Dating the onset of cataract. Trans. Ophthalmol. Soc. U. K. 1976; 96:18–23. [PubMed: 1070853]

Brown N. Cataract in childhood: photograph methods in assessment. Br. J. Ophthalmol. 1977; 61:135–140. [PubMed: 843511]

Brown NA, Sparrow JM, Bron AJ. Central compaction in the process of lens growth as indicated by lamellar cataract. Br. J. Ophthalmol. 1988; 72:538–544. [PubMed: 3415946]

Campbell MC. Measurement of refractive index in an intact crystalline lens. Vis. Res. 1984; 24:409–415. [PubMed: 6740962]

Castoro JA, Bettelheim FA. Distribution of the total and non-freezable water in rat lenses. Exp. Eye Res. 1986; 43:185–191. [PubMed: 3758218]

Costello MJ, McIntosh TJ, Robertson JD. Membrane specializations in mammalian lens fiber cells: distribution of square arrays. Curr. Eye Res. 1985; 4:1183–1201. [PubMed: 4075818]

Costello MJ, McIntosh TJ, Robertson JD. Distribution of gap junctions and square array junctions in the mammalian lens. Invest. Ophthalmol. Vis. Sci. 1989; 30:975–989. [PubMed: 2722452]

Costello MJ, Mohamed A, Gilliland KO, Fowler WC, Johnsen S. Ultra-structural analysis of the human lens fiber cell remodeling zone and the initiation of cellular compaction. Exp. Eye Res. 2013; 116:411–418. [PubMed: 24183661]

David LL, Azuma M, Shearer TR. Cataract and the acceleration of calpain-induced beta-crystallin insolubilization occurring during normal maturation of rat lens. Invest. Ophthalmol. Vis. Sci. 1994; 35:785–793. [PubMed: 8125740]

De Maria A, Shi Y, Kumar NM, Bassnett S. Calpain expression and activity during lens fiber cell differentiation. J. Biol. Chem. 2009; 284:13542–13550. [PubMed: 19269960]

Dickson DH, Crock GW. Interlocking patterns on primate lens fibers. Invest. Ophthalmol. 1972; 11:809–815. [PubMed: 4627255]

Dubbelman M, Van der Heijde GL. The shape of the aging human lens: curvature, equivalent refractive index and the lens paradox. Vis. Res. 2001; 41:1867–1877. [PubMed: 11369049]

Ebihara L, Korzyukov Y, Kothari S, Tong JJ. Cx46 hemichannels contribute to the sodium leak conductance in lens fiber cells. Am. J. Physiol. Cell Physiol. 2014; 306:C506–C513. [PubMed: 24380846]

Faulkner-Jones B, Zandy AJ, Bassnett S. RNA stability in terminally differentiating fibre cells of the ocular lens. Exp. Eye Res. 2003; 77:463–476. [PubMed: 12957145]

Freel CD, al-Ghoul KJ, Kuszak JR, Costello MJ. Analysis of nuclear fiber cell compaction in transparent and cataractous diabetic human lenses by scanning electron microscopy. BMC Ophthalmol. 2003; 3:1. [PubMed: 12515578]

Gao J, Sun X, Moore LC, Brink PR, White TW, Mathias RT. The effect of size and species on lens intracellular hydrostatic pressure. Invest. Ophthalmol. Vis. Sci. 2013; 54:183–192. [PubMed: 23211824]

Gao J, Sun X, Moore LC, White TW, Brink PR, Mathias RT. Lens intracellular hydrostatic pressure is generated by the circulation of sodium and modulated by gap junction coupling. J. Gen. Physiol. 2011; 137:507–520. [PubMed: 21624945]

Gao J, Sun X, White TW, Delamere NA, Mathias RT. Feedback regulation of intracellular hydrostatic pressure in surface cells of the lens. Biophys. J. 2015; 109:1830–1839. [PubMed: 26536260]

Gladstone JH, Dale TP. Researches on the refraction, dispersion and sensitiveness of liquids. Philos. Trans. R. Soc. Lond. 1864; 153:317–343.

Glasser A, Campbell MC. Biometric, optical and physical changes in the isolated human crystalline lens with age in relation to presbyopia. Vis. Res. 1999; 39:1991–2015. [PubMed: 10343784]

Harding CV, Hughes WL, Bond VP, Schork P. Autoradiographic localization of tritiated thymidine in wholemount preparations of lens epithelium. Arch. Ophthalmol. 1960; 63:58–65. [PubMed: 14399723]

Hoshino M, Uesugi K, Yagi N, Mohri S, Regini J, Pierscionek B. Optical properties of in situ eye lenses measured with X-ray Talbot interferometry: a novel measure of growth processes. PLoS One. 2011; 6:e25140. [PubMed: 21949870]

Jones CE, Atchison DA, Meder R, Pope JM. Refractive index distribution and optical properties of the isolated human lens measured using magnetic resonance imaging (MRI). Vis. Res. 2005; 45:2352–2366. [PubMed: 15979462]

Kenworthy AK, Magid AD, Oliver TN, McIntosh TJ. Colloid osmotic pressure of steer alpha- and beta-crystallins: possible functional roles for lens crystallin distribution and structural diversity. Exp. Eye Res. 1994; 59:11–30. [PubMed: 7835391]

Kreuzer RO, Sivak JG. Spherical-aberration of the fish lens – interspecies variation and age. J. Comp. Physiol. 1984; 154:415–422.

Kuszak J, Alcala J, Maisel H. The surface morphology of embryonic and adult chick lens-fiber cells. Am. J. Anat. 1980; 159:395–410. [PubMed: 7223675]

Kuszak, JR., Costello, MJ. Structure of the vertebrate lens. In: Lovicu, FJ., Robinson, ML., editors. Development of the Ocular Lens. Cambridge: Cambridge University Press; 2004.

Kuszak JR, Ennesser CA, Umlas J, Macsai-Kaplan MS, Weinstein RS. The ultrastructure of fiber cells in primate lenses: a model for studying membrane senescence. J. Ultrastruct. Mol. Struct. Res. 1988; 100:60–74. [PubMed: 3209860]

Kuszak JR, Zoltoski RK, Sivertson C. Fibre cell organization in crystalline lenses. Exp. Eye Res. 2004; 78:673–687. [PubMed: 15106947]

Kuwabara T. The maturation of the lens cell: a morphologic study. Exp. Eye Res. 1975; 20:427–443. [PubMed: 1126408]

Lahm D, Lee LK, Bettelheim FA. Age dependence of freezable and non-freezable water content of normal human lenses. Invest. Ophthalmol. Vis. Sci. 1985; 26:1162–1165. [PubMed: 4019108]

Lim JC, Walker KL, Sherwin T, Schey KL, Donaldson PJ. Confocal microscopy reveals zones of membrane remodeling in the outer cortex of the human lens. Invest. Ophthalmol. Vis. Sci. 2009; 50:4304–4310. [PubMed: 19357350]

Lo WK, Biswas SK, Brako L, Shiels A, Gu S, Jiang JX. Aquaporin-0 targets interlocking domains to control the integrity and transparency of the eye lens. Invest. Ophthalmol. Vis. Sci. 2014; 55:1202–1212. [PubMed: 24458158]

Lo WK, Harding CV. Square arrays and their role in ridge formation in human lens fibers. J. Ultrastruct. Res. 1984; 86:228–245. [PubMed: 6544861]

Ma H, Hata I, Shih M, Fukiage C, Nakamura Y, Azuma M, Shearer TR. Lp82 is the dominant form of calpain in young mouse lens. Exp. Eye Res. 1999; 68:447–456. [PubMed: 10192802]

Ma H, Shih M, Hata I, Fukiage C, Azuma M, Shearer TR. Protein for Lp82 calpain is expressed and enzymatically active in young rat lens. Exp. Eye Res. 1998; 67:221–229. [PubMed: 9733588]

Mathias RT. Steady-state voltages, ion fluxes, and volume regulation in syncytial tissues. Biophys. J. 1985; 48:435–448. [PubMed: 2412605]

Mathias RT, Kistler J, Donaldson P. The lens circulation. J. Membr. Biol. 2007; 216:1–16. [PubMed: 17568975]

Mathias RT, White TW, Gong X. Lens gap junctions in growth, differentiation, and homeostasis. Physiol. Rev. 2010; 90:179–206. [PubMed: 20086076]

McAvoy JW. Cell division, cell elongation and distribution of alpha-, beta- and gamma-crystallins in the rat lens. J. Embryol. Exp. Morphol. 1978; 44:149–165. [PubMed: 650132]

Mochizuki T, Masai I. The lens equator: a platform for molecular machinery that regulates the switch from cell proliferation to differentiation in the vertebrate lens. Dev. Growth Differ. 2014; 56:387–401. [PubMed: 24720470]

Moffat BA, Atchison DA, Pope JM. Age-related changes in refractive index distribution and power of the human lens as measured by magnetic resonance micro-imaging in vitro. Vis. Res. 2002; 42:1683–1693. [PubMed: 12079796]

Mutti DO, Zadnik K, Adams AJ. The equivalent refractive index of the crystalline lens in childhood. Vis. Res. 1995; 35:1565–1573. [PubMed: 7667914]

Patterson JW, Fournier DJ. The effect of tonicity on lens volume. Invest. Ophthalmol. 1976; 15:866–869. [PubMed: 977257]

Philipson B. Distribution of protein within the normal rat lens. Invest. Ophthalmol. 1969; 8:258–270. [PubMed: 5772717]

Pierscionek B, Bahrami M, Hoshino M, Uesugi K, Regini J, Yagi N. The eye lens: age-related trends and individual variations in refractive index and shape parameters. Oncotarget. 2015; 6:30532–30544. [PubMed: 26416418]

Pierscionek B, Smith G, Augusteyn RC. The refractive increments of bovine alpha-, beta-, and gamma-crystallins. Vis. Res. 1987; 27:1539–1541. [PubMed: 3445487]

Pierscionek BK. Refractive index of the human lens surface measured with an optic fibre sensor. Ophthalmic Res. 1994; 26:32–35. [PubMed: 8134087]

Pierscionek BK. Refractive index contours in the human lens. Exp. Eye Res. 1997; 64:887–893. [PubMed: 9301469]

Pierscionek BK, Belaidi A, Bruun HH. Optical development in the foetal bovine lens. Exp. Eye Res. 2003; 77:639–641. [PubMed: 14550406]

Pierscionek BK, Regini JW. The gradient index lens of the eye: an optobiological synchrony. Prog. Retin Eye Res. 2012; 31:332–349. [PubMed: 22465790]

Rafferty NS, Smith R. Analysis of cell-populations of Normal and injured mouse lens epithelium .1. Cell-cycle. Anat. Rec. 1976; 186:105–113.

Shi Y, De Maria A, Lubura S, Sikic H, Bassnett S. The penny pusher: a cellular model of lens growth. Invest. Ophthalmol. Vis. Sci. 2015; 56:799–809.

Shi Y, Tu Y, De Maria A, Mecham RP, Bassnett S. Development, composition, and structural arrangements of the ciliary zonule of the mouse. Invest. Ophthalmol. Vis. Sci. 2013; 54:2504–2515. [PubMed: 23493297]

Shih M, Lampi KJ, Shearer TR, David LL. Cleavage of beta crystallins during maturation of bovine lens. Mol. Vis. 1998; 4:4. [PubMed: 9485487]

Siebinga I, Vrensen GF, De Mul FF, Greve J. Age-related changes in local water and protein content of human eye lenses measured by Raman microspectroscopy. Exp. Eye Res. 1991; 53:233–239. [PubMed: 1915680]

Sikic H, Shi Y, Lubura S, Bassnett S. A stochastic model of eye lens growth. J. Theor. Biol. 2015; 376:15–31. [PubMed: 25816743]

Sivak JG, West JA, Campbell MC. Growth and optical development of the ocular lens of the squid (Sepioteuthis lessoniana). Vis. Res. 1994; 34:2177–2187. [PubMed: 7941414]

Smith P. A further investigation of the pathology of glaucoma. R. Lond. Ophthalmic Hosp. Rep. 1882; 10:25–43.

Smith P. On the growth of the crystalline lens. Trans. Ophthalmol. Soc. U. K. 1883; 3:79–99.

Stirling RJ, Wakely J. Changes in the surface morphology of lens fibres in the developing chick eye in relation to lens transparency. J. Anat. 1987; 155:11–22. [PubMed: 3503044]

Takamura Y, Kubo E, Tsuzuki S, Akagi Y. Apoptotic cell death in the lens epithelium of rat sugar cataract. Exp. Eye Res. 2003; 77:51–57. [PubMed: 12823987]

Taylor VL, al-Ghoul KJ, Lane CW, Davis VA, Kuszak JR, Costello MJ. Morphology of the normal human lens. Invest. Ophthalmol. Vis. Sci. 1996; 37:1396–1410. [PubMed: 8641842]

Ueda Y, Fukiage C, Shih M, Shearer TR, David LL. Mass measurements of C-terminally truncated alpha-crystallins from two-dimensional gels identify Lp82 as a major endopeptidase in rat lens. Mol. Cell Proteom. 2002; 1:357–365.

Vaghefi E, Kim A, Donaldson PJ. Active maintenance of the gradient of refractive Index is required to sustain the optical properties of the lens. Invest. Ophthalmol. Vis. Sci. 2015; 56:7195–7208. [PubMed: 26540658]

Vaghefi E, Pontre BP, Jacobs MD, Donaldson PJ. Visualizing ocular lens fluid dynamics using MRI: manipulation of steady state water content and water fluxes. Am. J. Physiol. Regul. Integr. Comp. Physiol. 2011; 301:R335–R342. [PubMed: 21593426]

Veretout F, Delaye M, Tardieu A. Molecular basis of eye lens transparency. Osmotic pressure and X-ray analysis of alpha-crystallin solutions. J. Mol. Biol. 1989; 205:713–728. [PubMed: 2926823]

Veretout F, Tardieu A. The protein concentration gradient within eye lens might originate from constant osmotic pressure coupled to differential interactive properties of crystallins. Eur. Biophys. J. 1989; 17:61–68. [PubMed: 2766998]

Vrensen G, Van Marle J, Van Veen H, Willekens B. Membrane architecture as a function of lens fibre maturation: a freeze fracture and scanning electron microscopic study in the human lens. Exp. Eye Res. 1992; 54:433–446. [PubMed: 1521571]

Willekens B, Vrensen G. Lens fiber organization in four avian species: a scanning electron microscopic study. Tissue Cell. 1985; 17:359–377. [PubMed: 4012767]

Wilmarth PA, Taube JR, Riviere MA, Duncan MK, David LL. Proteomic and sequence analysis of chicken lens crystallins reveals alternate splicing and translational forms of beta B2 and beta A2 crystallins. Invest. Ophthalmol. Vis. Sci. 2004; 45:2705–2715. [PubMed: 15277495]

Wistow G, Piatigorsky J. Recruitment of enzymes as lens structural proteins. Science. 1987; 236:1554–1556. [PubMed: 3589669]

Wu JJ, Wu W, Tholozan FM, Saunter CD, Girkin JM, Quinlan RA. A dimensionless ordered pull-through model of the mammalian lens epithelium evidences scaling across species and explains the age-dependent changes in cell density in the human lens. J. R. Soc. Interface. 2015; 12:20150391. [PubMed: 26236824]

Yorio T, Bentley PJ. Distribution of the extracellular space of the amphibian lens. Exp. Eye Res. 1976; 23:601–608. [PubMed: 826402]

Zampighi G, Simon SA, Robertson JD, McIntosh TJ, Costello MJ. On the structural organization of isolated bovine lens fiber junctions. J. Cell Biol. 1982; 93:175–189. [PubMed: 7068755]

Zampighi GA, Hall JE, Ehring GR, Simon SA. The structural organization and protein composition of lens fiber junctions. J. Cell Biol. 1989; 108:2255–2275. [PubMed: 2738093]

Zhao H, Brown PH, Magone MT, Schuck P. The molecular refractive function of lens gamma-crystallins. J. Mol. Biol. 2011a; 411:680–699. [PubMed: 21684289]

Zhao H, Brown PH, Schuck P. On the distribution of protein refractive index increments. Biophys. J. 2011b; 100:2309–2317. [PubMed: 21539801]

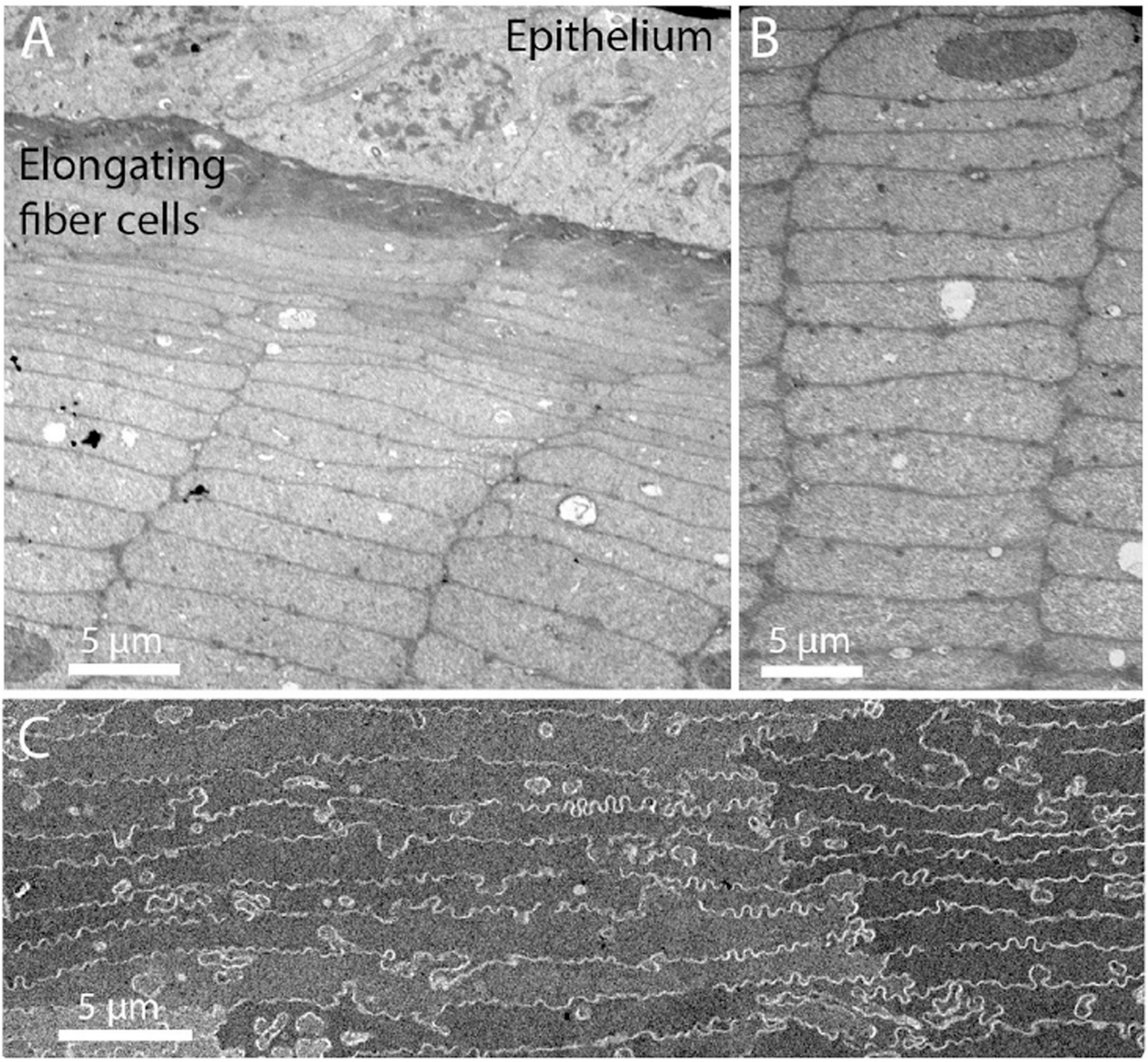

Fig. 1.

Fiber cell compaction in the outer layers of aged human lenses. A. Overview showing epithelial cells and cross-sectioned elongating fiber cells. B. Fiber cells in a radial cell column about 40 µm beneath the lens capsule. Note the flattened hexagonal cell profiles. Average cell thickness is about 2 µm. C. Compacted cells in the adult nucleus about 750 µm from the capsule showing undulating membranes that correspond to the microplicae seen in scanning electron micrographs of this region. The average fiber cell thickness is about 0.6 µm. Electron micrographs are from transparent human donor lenses about 60 years old prepared as described (Costello et al., 2013).